

Switchable up and down-conversion luminescent properties of Nd (III)-nanopaper for visible and near-infrared anti-counterfeiting

Zhao Zhang^{a,b,*}, Ningning Ma^a, Xiena Kang^a, Xinping Li^{a,*}, Shuangquan Yao^{c,**}, Wenjia Han^d, Hui Chang^e

^a College of Bioresources Chemical and Materials Engineering, National Demonstration Center for Experimental Light Chemistry Engineering Education, Shaanxi University of Science and Technology, Xi'an, 710021, Shaanxi, PR China

^b State Key Laboratory of Pulp and Paper Engineering, South China University of Technology, Guangzhou, 510640, PR China

^c Guangxi Key Laboratory of Clean Pulp & Papermaking and Pollution Control, College of Light Industry and Food Engineering, Guangxi University, Nanning, 530004, PR China

^d State Key Laboratory of Biobased Material and Green Papermaking, Qilu University of Technology, Shandong Academy of Sciences, Jinan, 250353, PR China

^e College of Mechanical and Electrical Engineering, Shaanxi University of Science and Technology, Xi'an, 710021, PR China

ARTICLE INFO

Keywords:

Lanthanide-base cellulose nanopaper
Down-conversion NIR luminescence
Up-conversion visible emission
Fluorescent brighteners
High level anti-counterfeiting

ABSTRACT

A series of lanthanide-based nanopaper (Nd-nanopaper) was synthesized via a neodymium organic framework (Nd-MOFs)-grafted TEMPO-oxidized cellulose nanofibrils (tCNF) using a solvothermal reaction. Not using the traditional down-conversion visible emissions of anti-counterfeiting techniques, this Nd-nanopaper achieved down-conversion near-infrared (NIR) and up-conversion visible emissions. The down-conversion luminescent property of these Nd-nanopapers exhibited characteristic NIR luminescence ($\lambda_{Em} = 1080$ nm) of Nd³⁺ ions with 311 nm excitation, undergoing an "antenna" effect. In contrast, the up-conversion visible light emission ($\lambda_{Em} = 450$ nm) of Nd-nanopaper was detected under 580 nm excitation. The mechanism of up-conversion fluorescence was ascribed to excited-state absorption and energy transfer up-conversion. Interestingly, Nd-nanopaper induced both up and down-conversions for visible and NIR emissions that were completely devoid of the interference from fluorescent brighteners and background fluorescence. These switchable up and down-conversion fluorescent Nd-nanopapers with visible and NIR dual emissions or dual channels could be applied in high level anti-counterfeiting applications.

1. Introduction

With the continuous advancement of society, counterfeit and shoddy products are mixed into daily life (Andres, Hersch, Moser, & Chauvin, 2014). Counterfeits of paper products, such as banknotes, passports, patents, and documents from all over the world, not only harm the interests of individuals and businesses but also endanger national security (Kaczmarek et al., 2017; Resch-Genger, 2020). Governments and businesses around the world have spent much resources, time, and energy to protect the results and products of their intellectual property owners. At present, researchers have developed many paper-based anti-counterfeiting technologies, such as watermarks and thermal, holographic, and fluorescent anti-counterfeiting technology (Arppe & Sørensen, 2017; Jin

et al., 2018; Li et al., 2017; Wang et al., 2020; Zhang, Liu, Chang, Li, & Zhang, 2019; Zhang, Chen, Sun, Zhang, & Zhao, 2019). Among these anti-counterfeiting technologies, fluorescent materials have been widely studied because of their advantages of easy identification and permanent reversibility (Zhang, Liu et al., 2019, 2019b).

Fluorescent materials based on organic dyes (Leng, Jakubek, Mazloumi, Leung, & Johnston, 2017), carbon dots (Jing et al., 2015; Jiang et al., 2016), and quantum dots (Zhu et al., 2012) have been widely reported and used extensively to produce hybrid cellulose paper or nanopaper for visible (Vis) emission anti-counterfeiting applications. Vis anti-counterfeiting takes advantages of naked-eye recognition, with a low security level that is easily imitated. In recent years, lanthanide-based materials have attracted attention due to the excellent

* Corresponding authors at: College of Bioresources Chemical and Materials Engineering, National Demonstration Center for Experimental Light Chemistry Engineering Education, Shaanxi University of Science and Technology, Xi'an, 710021, Shaanxi, PR China.

** Corresponding author.

E-mail addresses: zhangzhaogq@sust.edu.cn (Z. Zhang), lixp@sust.edu.cn (X. Li), yaoshuangquan@gxu.edu.cn (S. Yao).

<https://doi.org/10.1016/j.carbpol.2020.117134>

Received 23 July 2020; Received in revised form 6 September 2020; Accepted 18 September 2020

Available online 29 September 2020

0144-8617/© 2020 Elsevier Ltd. All rights reserved.

luminescence of lanthanide (Ln^{3+}) ions, large Stokes shifts, line-shaped spectra and microsecond lifetime (Wang, Batentschuk, Osvet, Pinna, & Brabec, 2011). In particular, Nd^{3+} , Yb^{3+} , and Er^{3+} ions extend emissions to the near-infrared (NIR) regions or emit Vis light through up-conversion, which greatly improves anti-counterfeiting characteristics. Zhao et al. have obtained nanopapers with up-conversion luminescence characteristics for anti-counterfeiting using cellulose nanofibrils (CNFs) doped with $\text{NaYF}_4:\text{Yb}$, Er nanoparticles (Zhao et al., 2014). You et al. have reported lanthanide up-conversion fluorescence based on 3D quick response (QR) codes fabricated by inkjet printing technology for drug anti-counterfeiting (You et al., 2016). Da Luz et al. have demonstrated photoluminescent lanthanide-organic frameworks (Ln-MOFs) printed onto flexible substrates (paper and plastic foils) with a conventional inkjet printer (Da Luz et al., 2015). To date, there appear to have been few reports on the development of lanthanide-based materials with dual-emission mixed (dual-channel) fluorescence for anti-counterfeiting. On the other hand, these lanthanide-based fluorescent materials doped into or coated/printed onto nanopaper, give rise to poor stability and easy response losses. The fluorescent material modification of nanocellulose via coordination, covalent, or ionic bonds is helpful for improving material stability and, in comparison, coordination bond-modified nanocellulose is simple and the driving force of the reactions comes from coordination abilities between Ln^{3+} ions and coordination sites (Miao et al., 2015). It is very interesting to use Ln-MOF -coordinate bonding TEMPO-oxidized CNF (tCNF) for preparing Vis and NIR dual-emission mixed dual-channel anti-counterfeiting materials (Gao, Han, & Wang, 2018; Liu, Ai, & Lu, 2011).

In this study, Nd-MOFs with up and down-conversion luminescent characteristics were first prepared and then grafted to tCNF using a solvothermal reaction. After coordinate bond coupling of tCNF carboxyl group and lanthanide ions, a heterogeneous network structure was formed, thereby preparing a series of fluorescent nanopapers via Buchner funnel filtering. This novel up-conversion Vis and down-conversion NIR emission nanopaper successfully avoided the emission range of fluorescent brighteners, and these dual channels could be switched via excitation control. In addition, fluorescent brighteners in Nd-nanopaper@FB achieved down-conversion Vis emission, that offering a dual emission system with Nd-nanopaper 's down-conversion NIR emission. This dual emission and dual-channel anti-counterfeiting system within nanopaper could further improve the security of anti-counterfeiting (Fig. 1).

2. Experimental section

2.1. Materials

The needle bleached kraft pulp (NBKP) is purchased from Tianjin Woodlf Biotechnology Co., Ltd. The main ingredients of NBKP are cellulose (65.5 %) and hemicelluloses (31.5 %), which also contain a small amount of lignin (1.8 %). N, N-dimethylformamide was purchased from Sinopharm Co., Ltd. Sodium bromide (NaBr , AR), sodium hypochlorite (NaClO , AR), absolute ethanol (CH_3COOH , AR), glacial acetic acid (CH_3COOH , AR), acetone (CH_3COCH_3 , AR), sulfuric acid (H_2SO_4 , 98 %) and potassium hydroxide (KOH , AR) was purchased from Kermel Chemical Reagents Co., Ltd (Tianjin, China). Reagents grade, $\text{NdCl}_3 \cdot 6\text{H}_2\text{O}$ and 1,3,5-Benzenetricarboxylic acid (H_3BTC) were purchased from Aladdin Reagents Co., Ltd (Shanghai, China) and 2,2,6,6-tetramethyl-piperidine-1-oxyl (TEMPO, 98 %) bought from Sigma-Aldrich Inc (St. Louis, MO, USA). All chemicals were used without any further purification. All coordination polymers were formed in a Teflon-lined stainless-steel vessel under autogenous pressure and afterward gradually cooled to room temperature.

2.2. Synthesis of Nd-MOFs

A mixture of $\text{NdCl}_3 \cdot 6\text{H}_2\text{O}$ (0.006 mmol), H_3BTC (0.02 mmol), N,N-dimethylformamide (10 mL), and deionized water (10 mL) were well mixed in a sealed vial. Then, the vial was heated at 115 °C for 8 h. The final purple product $[\text{Nd}(\text{BTC})] \cdot (\text{H}_2\text{O})$ (Nd-MOFs) were separated by filtration, washed with ethanol, and then dried under vacuum at 80 °C for 12 h.

2.3. Preparation of tCNF

According to the literature, this method mainly induces the oxidation of C6-aldehyde groups of CNFs to C6-carboxyl groups via the TEMPO/ NaBr/NaClO oxidation system (Chen, Geng, Jing, Tong, & Chen, 2017). First, a quantitative amount of needle bleached kraft pulp (NBKP) were dispersed in aqueous solution and subjected to ultrasonic treatment. In addition, a mixed aqueous NBKP dispersion system was obtained by adding a certain ratio of aqueous solutions of TEMPO and NaBr aqueous solution. The pH was adjusted to 10.5 by adding KOH solution to the above solution, with NaClO solution gradually added as an oxidizing agent, to carry out the oxidation reaction, and stirred for 3 h. Finally, the pH was adjusted to 7 using hydrochloric acid to prepare oxidized tCNF

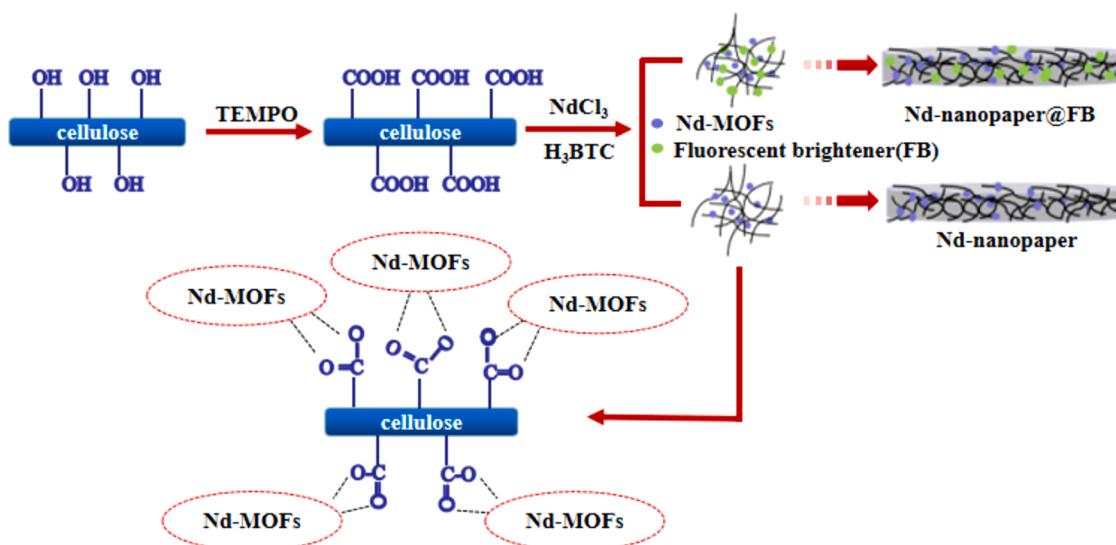


Fig. 1. Schematic diagram for the preparation of Nd-nanopaper and Nd-nanopaper@FB .

and the obtained suspension filtered and washed with pure water and subjected to high pressure homogenization 20 times to obtain a uniform tCNF suspension. The main ingredients of tCNF were cellulose (81.81 %) and hemicelluloses (14.94 %), with a small amount of lignin (0.78%). Further, the surface charge (-1.59×10^{-3} eq/g) of tCNF was determined using a colloidal charge titrator.

2.4. Preparation of Nd-MOFs-grafted-nanopaper

A mixture of $\text{NdCl}_3 \cdot 6\text{H}_2\text{O}$ (0.06 mmol), 1,3,5-benzenetricarboxylic acid (H_3BTC , 0.02 mmol), tCNF (2.5 mL), and deionized water (10 mL) were evenly added to a sealed vial. The reaction vessel was heated at 105 °C for 3 h and the resulting suspension filtered to prepare Nd-MOFs-grafted-nanopaper (Nd-nanopaper) using Buchner funnel filtering. Then, the Nd-nanopaper was peeled off the filter, pressed between smooth glass plates, and allowed to dry naturally at ambient atmosphere for 24 h.

2.5. Preparation of Nd-nanopaper encapsulated fluorescent brighteners

Based on the Nd-nanopapers described above, a series of Nd-nanopaper encapsulated fluorescent brighteners (Nd-nanopaper@FB) were prepared using a similar method. The fluorescent brighteners were 1,1'-biphenyl-4,4'-bis[2-(methoxyphenyl)ethenyl] (FB-1), 4,4-bis(5-methyl-2-benzoxazol)-ethylene (FB-2), 1,4-bis(benziazolyl-2-yl)-naphthalene (FB-3), 4,4'-(2-sulfostyryl)biphenyl disodium (FB-4), 4,4'-bis(2-benzoxazolyl)-stilbene (FB-5), 4,4'-(1,4-phenylenebis(ethene-2,1-dyl)) (FB-6), and 2,5-bis(5-tert-butyl-benzoxazol-2-yl)thiophene (FB-7). A mixture of $\text{NdCl}_3 \cdot 6\text{H}_2\text{O}$ (0.06 mmol), H_3BTC (0.1 mmol), tCNF (2.5 mL), and deionized water (10 mL) was well mixed in a sealed vial. Then, 4.26 mg of fluorescent brighteners were dissolved in DMF (1 mL) and added to the above solution. Finally, the reaction vessel was heated at 105 °C for 3 h, the aqueous suspension filtered to prepare Nd-nanopaper using Buchner funnel filtering, and the product washed three times with alternating water and ethanol. Then, the Nd-nanopaper@FB was peeled off, pressed between smooth glass plates, and allowed to dry naturally at ambient atmosphere for 24 h.

3. Results and discussion

3.1. Preparation and characterization of Nd-nanopaper and Nd-nanopaper@FB

The tCNF was prepared by TEMPO-mediated oxidization of NBKP. Subsequently, Nd-MOFs were assembled on tCNF surfaces via coordinate bonding and then Nd-nanopaper produced by filtering with a Buchner funnel. Wide-angle powder X-ray diffractometric analysis (PXRD) was performed on Nd-MOFs, pristine nanopaper, and Nd-nanopaper. The resulting XRD patterns showed Nd-MOFs with sharp peaks present at 10.12, 16.8, 17.3, 29.2, and 33.8°, which indicated a crystalline material (Fig. 1S). In their PXRD patterns, pristine nanopapers showed peaks at 15.6 (110) and 22.8° (002), which were attributed to the crystalline structure of tCNF (Lin & Dufresne, 2014). Nd-nanopapers showed the prominent peaks at 15.6, 22.8, 29.2, and 33.8°, illustrating that Nd-nanopapers were composed of a combination of Nd-MOFs and pristine nanopaper. The crystallinity index of pristine (67%) and Nd-nanopapers (51 %) were calculated using the equation $I_c = 1 - I_1/I_2$, where I_1 is the amorphous region diffraction intensity $2\theta = 18^\circ$ and I_2 the intensity at $2\theta = 22.8^\circ$, related to the ordered (crystalline) area of tCNF (Abraham et al., 2016). These results indicated that the obtained Nd-MOFs were successfully combined with tCNF (Missoum, Bras, & Belgacem, 2012) and, by virtue of Nd-MOFs binding occurring solely at tCNF surfaces, tCNF crystalline structure was preserved.

FT-IR spectra of Nd-nanopaper, Nd-MOFs, and nanopaper demonstrated characteristic signal peaks at 3341 and 2901 cm^{-1} , which were attributed to stretching vibrations of -OH groups and C-H, respectively

(Fig. S2). For Nd-nanopaper, the absorption peak at 1620 cm^{-1} was due to stretching vibrations of tCNF carboxyl (C=O) groups. The peak at 1620 cm^{-1} was red-shifted by 20 cm^{-1} compared to pure tCNF (nanopaper), which was attributed to coordination of carboxyl groups and lanthanide ions and suggested coupling reactions between tCNF and Nd-MOFs. Therefore, FT-IR results demonstrated that Nd-MOFs had been coordinate-bonded with tCNF, resulting in the formation of Nd-nanopaper. By analyzing FT-IR spectra of Nd-nanopaper@FB, the broad band at 3412 cm^{-1} was assigned to O-H stretching vibrations and the band at 1616 cm^{-1} to COO^- stretching (Fig. S3). Furthermore, the peak located at 1350 cm^{-1} was assigned to stretching vibrations of C-H and the band at 1028 cm^{-1} to O-H in-plane bending vibrations. These results were basically consistent with the position of absorption peaks of Nd-nanopaper IR spectra. Therefore, the addition of fluorescent brightener was just impregnation into the nanopaper without chemical reaction and new bond formation. It also did not affect peak positions in the present Nd-nanopaper IR spectrum.

The dispersion uniformity of fluorescent brighteners in nanopaper is particularly important, because it determines the luminescence uniformity. Laser scanning confocal microscopy (LSCM) images showed that fluorescent dots distribution was relative uniform (Fig. S4), indicating that fluorescent brighteners were evenly distributed in the nanopaper. As the fluorescent brighteners were just associated in the Nd-nanopaper without any chemical reaction, therefore, its concentration in the nanopaper was determined via an external standard method. The absorbance curves at 5 different concentrations for each fluorescent brightener and standard curves of 7 kinds of fluorescent brighteners were obtained (Fig. S5). A 2.1 mg mass of Nd-nanopaper@FB was dispersed into 9 mL of solvent (Nd-nanopaper@FB1-6 DMF and Nd-nanopaper@FB7 H_2O) and their maximum absorbance measured. The fluorescent brightener content in the Nd-nanopaper@FB was calculated using the equation $y = ax + b$, where y is the absorbance and x the mass concentration. The coordinates of mass concentration and absorbance of the fluorescent brighteners were also noted and the mass concentration and absorbance of the seven Nd-nanopaper@FB nanopapers showed corresponding coordinates of Nd-nanopaper@FB1-(0.076, 0.89), Nd-nanopaper@FB2-(0.091, 0.72), Nd-nanopaper@FB3-(0.073, 0.85), Nd-nanopaper@FB4-(0.098, 0.95), Nd-nanopaper@FB5-(0.088, 0.76), Nd-nanopaper@FB6-(0.070, 0.87), and Nd-nanopaper@FB7-(0.118, 0.89).

For Nd-nanopapers, the homogeneous distribution of Nd-MOFs on the tCNF matrix played an important role in material photophysical properties. Images showed that Nd-MOF possessed tiny purple crystal particles with beautiful crystal clear luster (Fig. S6a). Further, the morphologies of Nd-MOFs was captured by scanning electron microscopic (SEM) images (Figs. S6b-S6c). Nd-MOFs were clearly seen to be rod-shaped, with 1–8 μm diameter and 15–90 μm length. Due to the influence of nano-size effects of tCNFs, there were no large-sized Nd-MOFs particles in Nd-nanopaper. As expected, Nd-nanopaper appeared dense and its surface smooth, which was similar to nanopaper (Fig. 2a and b). To our best knowledge, cellulose density was packed to form a layer-like structure and then layers connected by hydrogen bonds within the nanopaper. Through cross-sectional analysis, the layers between nanopaper and Nd-nanopaper sections were found to be very compact, with Nd-nanopaper sections appearing a little rougher than nanopaper, which might be attributed to Nd-MOF grafted tCNFs destroying hydrogen bonds and affecting its layered structure (Fig. 2c and d).

The elemental composition of Nd-MOFs and Nd-nanopaper was determined by X-ray photoelectron spectroscopy (XPS) analysis. The XPS spectra of Nd-MOFs and Nd-nanopaper illustrated that Nd-MOFs and Nd-nanopaper had similar compositions, primarily of C, O, and Nd (Table 1, Fig. 3a). The high-resolution XPS spectrum of C-1s exhibited five peaks at about 282.5, 282.8, 283.1, 284.2, and 286.6 eV, which were attributed to C=C, C-C, C-O, O-C-O, and O=C-O, respectively (Fig. 3b, Wang et al., 2014; Zor, Alpaydin, Arici, Saglam, & Bingol, 2017). The analysis of O-1s illustrated that oxygen was divided into two peaks at 527.95 eV for O-Nd bonds and 529.25 eV for O-C

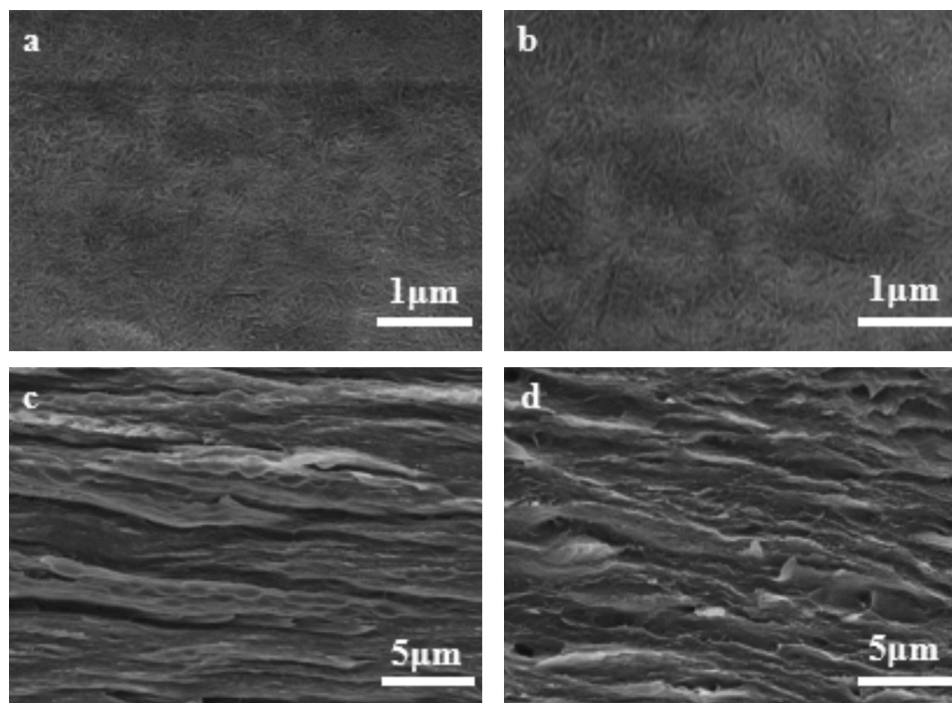


Fig. 2. SEM micrographs of nanopaper (a) and Nd-nanopaper (b) in the dispersion state (scale bar = 1 μm); the fracture surface of nanopaper (c) and Nd-nanopaper (d) (scale bar = 5 μm).

Table 1
Specific elemental data of Nd-MOFs and Nd-nanopaper.

Classification	Name	Binding Energy/ eV	FWHM/ eV	Area	At%
Nd-MOFs	C 1 s	283.00	2.872	334566.22	73.85
	O 1 s	530.00	3.215	258453.48	19.47
	Nd 3d	1003.00	5.871	30253.25	6.68
Nd-nanopaper	C 1 s	283.00	3.567	349267.06	69.77
	O 1 s	530.00	3.184	398007.11	27.14
	Nd 3d	1003.00	2.867	15462.57	3.09

bonds (Fig. 3c). These results confirmed the presence of oxygen-containing groups in the prepared Nd-MOFs, including $-\text{COOH}$ and $-\text{OH}$, which was in good agreement with FT-IR spectra. The C-1s peaks were deconvoluted into five parts at about 285.91, 286.41, 287.81, 288.61 and 290.01 eV and assigned to $\text{C}=\text{C}$, $\text{C}-\text{C}$, $\text{C}-\text{O}$, $\text{O}-\text{C}-\text{O}$, and $\text{O}=\text{C}-\text{O}$ respectively (Fig. 3d). The analysis of O-1s showed that oxygen was divided into three peaks at 532.86 eV for $\text{O}-\text{Nd}$ bonds, 531.26 eV for $\text{O}-\text{H}$ bonds, and 532.46 eV for $\text{O}-\text{C}$ bonds (Fig. 3e). In addition, high-resolution XPS spectra for Nd of Nd-MOFs and Nd-nanopaper were both concentrated at 1003.00 eV (Fig. 3f), which further confirmed the success of using trivalent state Nd^{3+} and indicated a higher tendency to form Nd-O bonds in Nd-MOFs and Nd-nanopaper.

Thermogravimetric, differential thermogravimetric, and differential scanning calorimetric (TG, DTG, and DSC, respectively) curves of samples are shown in the Supporting Information. For security anti-counterfeiting paper, good thermal stability is essential (Zhang, Chang et al., 2018; Zhang, Zhang et al., 2018). The thermal stabilities of Nd-MOFs, pristine nanopaper, and Nd-nanopaper were analyzed by TG curves (Fig. S7). Nd-MOFs exhibited a three-step thermal decomposition process, with the first stage, at $\sim 120^\circ\text{C}$, resulting in a weight loss of 24.6%. The polycrystalline structures lost DMF and H_2O when heated to 120°C and then remained stable, as a second stage, until the temperature reached 400°C . Additional thermal decomposition, the third stage,

appeared more complicated, appearing at ~ 400 and 520°C , which corresponded to the loss of organic compound groups and the formation of metal oxides. TG curves for Nd-nanopapers also showed a three-stage thermal decomposition process, with the first stage from 50 to 200°C with a small weight loss caused by water evaporation. In the second stage, the temperature range from 200 to 391°C , and it was decomposed rapidly at 345°C with a mass loss rate of $\sim 5.56\%/\text{min}$. A third stage exothermic enthalpy change at 391°C was observed in Nd-MOFs (Fig. S8). After assembly of Nd-MOFs on tCNF surfaces, a similar exothermic enthalpy change occurred for the material at 372°C , which was a 19°C decrease compared to Nd-MOFs alone. The third stage, from 391 to 600°C , resulted in the formation of residues due to the degradation of the nanocellulose backbone. Notably, the degradation temperature was very close to that of pristine nanopaper, which was distinctly shown from the DTG curves (Fig. S9). Compared with pristine nanopapers, Nd-nanopapers had higher residue amounts, which was likely to be related to the introduction of Nd-MOF centers. These TG-DTG-DSC results further indicated that Nd-nanopaper had excellent thermal stability from 0 to 200°C and could be used in security anti-counterfeiting paper.

3.2. Photophysical properties of Nd-MOFs and Nd-nanopaper

UV-Vis absorption spectra of samples showed that Nd-MOFs exhibited a narrow-band absorption peak corresponding to the $4f$ electron transition of Nd^{3+} ions in the range of 350 to 1000 nm (Fig. S10). There was one strong absorption peak in Nd-MOFs and Nd-nanopapers at 580 nm, which corresponded to the absorption transition of $^4\text{I}_{9/2} \rightarrow ^4\text{G}_{5/2}$. The strong absorption at wavelengths < 350 nm were attributed to the absorption of the H_3BTC ligand. Notably, Nd-MOFs exhibited a strong ligand $\pi-\pi^*$ absorption band at 200–350 nm, which showed a significant red shift compared with the free ligand $\pi-\pi^*$ absorption band, indicating that Nd-MOFs were formed. The conjugation and planarity of the post-substitution system appeared to be enhanced. At the same time, the main characteristic of Nd^{3+} was the characteristic absorption band from 350 to 1000 nm. In addition to the characteristic absorption of Nd-MOFs between 400 and 750 nm, Nd-nanopaper exhibited almost no

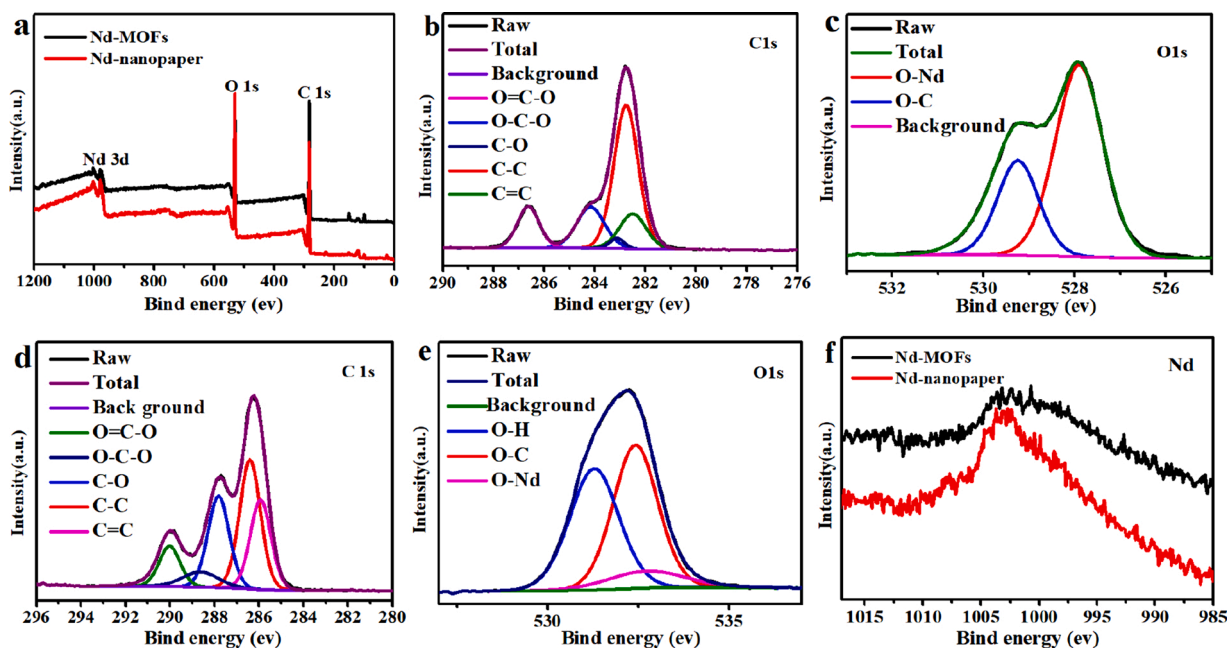


Fig. 3. XPS pattern of Nd-MOFs and Nd-nanopaper (a). The high-resolution XPS spectra of Nd-MOFs and Nd-nanopaper of C 1s (b) and (d), O 1s (c) and (e), Nd 3d (f), respectively.

other absorption peaks (Fig. S11). Compared with nanopaper, the light transmittance of Nd-nanopaper decreased slightly at 400 nm, which was attributed to the likely light absorption of Nd-MOFs and light scattering of the relatively rough nanopaper (Foster et al., 2018).

Photoluminescence (PL) spectra were utilized to investigate the luminescent properties of Nd-MOFs and Nd-nanopapers. The up and down-conversion PL spectra of Nd-nanopapers and Nd-MOFs are displayed in Figs. 4a and S12, respectively. The PL spectra of Nd-MOFs and Nd-nanopaper excited at 580 nm showed up-conversion fluorescence peaks both at 450 nm with a 5 nm half-band widths. At the same time, when 311 nm excited Nd-MOFs and Nd-nanopapers, light emission appeared in the NIR region. The corresponding down-conversion fluorescence peaks appeared at 903, 1060, and 1334 nm, and their distinct emission bands deduced to represent ${}^4F_{3/2} \rightarrow {}^4I_{9/2}$, ${}^4F_{3/2} \rightarrow {}^4I_{11/2}$, and ${}^4F_{3/2} \rightarrow {}^4I_{13/2}$ transitions of Nd^{3+} , respectively. Clearly, the appearance of the Nd^{3+} *f-f* emission band in Nd-MOF centers was due to more effective ligand sensitization to Nd^{3+} . In addition, the two emission bands of the Nd^{3+} at 1060 and 1334 nm were blue-shifted compared

with their theoretical values (1081 and 1379 nm), which was the result of the adjustment of the system's internal energy levels after formation of Nd-MOFs emitting centers (Lupei & Lupei, 2000).

3.3. Up- and down-conversion mechanisms of Nd-MOFs and Nd-nanopaper

The up and down-conversion PL mechanisms of Nd-MOFs and Nd-nanopaper were further studied by examining the energy transfer process of Nd-MOFs and Nd-nanopaper (Fig. 4b). In the final analysis, as the luminescence of Nd-nanopaper was Nd-MOF luminescence, only Nd-MOFs were discussed here. The electronic transition mechanisms of Nd-MOFs at different excitation wavelengths have been summarized, including 311, 580, and 808 nm for green, red, and yellow lines, respectively (Tai, Li, & Pan, 2018). The up-conversion luminescence mechanism has been studied in lanthanide ion systems, corresponding to the red line arrow. The present up-conversion luminescence mechanism was thus attributed to two explanations for excited state absorption

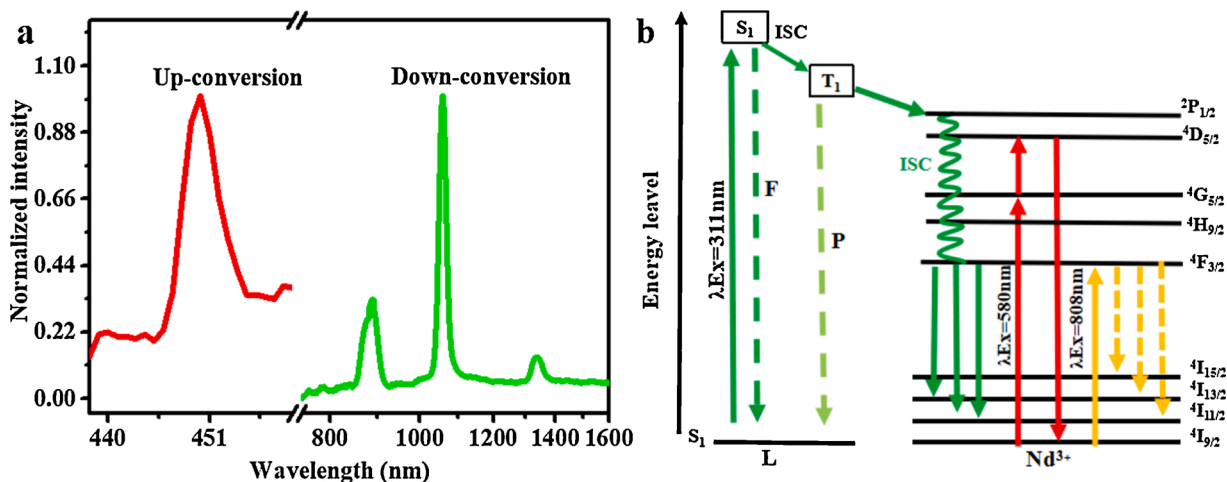


Fig. 4. Up-conversion and down-conversion fluorescence spectrum of Nd-nanopaper excited by 580 nm laser line and 311 nm laser line (a); energy level diagram for the fluorescent emission of the Nd-MOFs (b).

(ESA) and energy transfer up-conversion (ETU) (Chuang & Verdun, 1996; Courrol et al., 2004). The former was a single Nd^{3+} ion, which continuously absorbed two 580 nm photons and reached the $^4\text{D}_{5/2}$ energy level through the excited state energy of $^4\text{G}_{5/2}$. The higher the excited state energy level was, the more transitions back to the ground state that radiated photons. The latter involved two Nd^{3+} ions absorbing two 580 nm photons to reach the excited state of $^4\text{G}_{5/2}$, with one Nd^{3+} ion transferring energy to another Nd^{3+} ion and returning to ground state. Another Nd^{3+} ion received energy and jumped to a higher excited state, inducing up-conversion fluorescence ($\lambda_{\text{Em}} = 450$ nm), corresponding to the Nd^{3+} ion $^2\text{D}_{5/2} \rightarrow ^4\text{I}_{11/2}$ transition.

According to the solid sensitization theory of Dexter (1953) and the

maximum sensitization range of organic ligands ($\Delta E = 2100\text{--}3200$ cm^{-1}) proposed by Sato et al. (Sato & Wada, 1970), it was here known that the excited state energy level of the ligand must have been higher than the co-transfer of energy and occurred only when the excited state energy level was within a certain range. From the absorption and fluorescence emission spectra of Nd-MOFs, the ligand was concluded to have been effectively sensitized Nd^{3+} , which is the "antenna effect". This indicated that the triplet (T_1) energy level of the H_3BTC ligand of the transition to Nd^{3+} might have been effective. At this time, the ligand electrons returned from the lowest vibration energy level of the first excited singlet state S_1 to the optical radiation generated by the vibration energy levels of the ground state S_0 , which was fluorescence. When

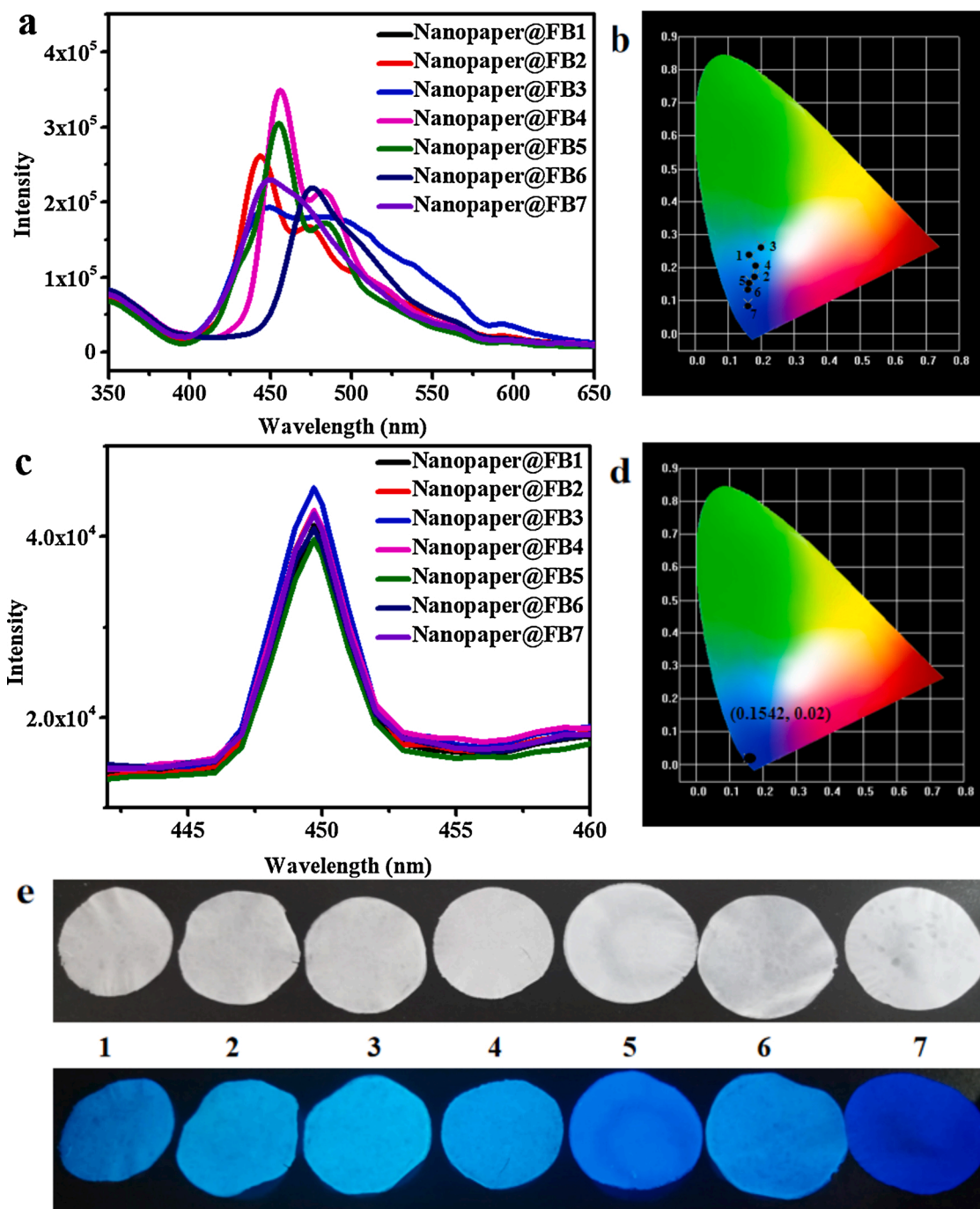


Fig. 5. Emission spectra (a) and CIE chromaticity graphs (b) of Nd-nanopaper@FB under 311 nm excitation; up-conversion fluorescence spectra (c) and CIE chromaticity graphs (d) of Nd-nanopaper@FB excited by 580 nm laser line; the photos of seven Nd-nanopaper@FB under natural light and UV-irradiation under 365 nm excitation (e).

the stimulated electron dropped to the lowest vibration energy level of S_1 , it did not emit fluorescence, but instead reached the T_1 vibration energy level through the intersystem transition (ISC) and relaxed to the lowest vibration energy level of T_1 after vibration relaxation, from the lowest vibration energy of T_1 . The optical radiation emitted by each vibration level back to the ground state was phosphorescence. Finally, the ligand transitioned the excited state energy to the ${}^2P_{1/2}$ excited state of Nd^{3+} . Then, for each energy level transition of Nd^{3+} , the down-conversion fluorescent emission energy level diagram of Nd-MOFs corresponded to the green line. The electronic energy level transition that converted the fluorescence ($\lambda_{Ex} = 311$ nm) to NIR were 903 nm for ${}^4F_{3/2} \rightarrow {}^4I_{9/2}$, 1060 nm for ${}^4F_{3/2} \rightarrow {}^4I_{11/2}$, and 1334 nm for ${}^4F_{3/2} \rightarrow {}^4I_{13/2}$.

3.4. NIR-visible dual emission and dual channel anti-counterfeiting of Nd-nanopapers under fluorescent brighteners environment

Fluorescent brighteners (Santos, Battle, Salafranca, & Nerín, 2005; Shu & Ding, 2009) appear very frequently in our daily lives, being widely used in a variety of applications in the textile, paper, detergent, and plastic industries. In the paper industry, fluorescent brighteners are one of the most important additives. Consequently, anti-counterfeiting nanopapers must avoid the effects of fluorescent brighteners. From the Vis light fluorescent spectrum of Nd-nanopaper@FB excited at a wavelength of 311 nm, it was inferred that there must be a down-conversion in the NIR fluorescent spectrum consistent with Nd-nanopaper nanoparticles ($\lambda_{max} = 1080$ nm, Fig. S13). Furthermore, Vis spectra were interpreted with the aid of Commission Internationale deL'Eclairage (CIE) chromaticity coordinates in a chromaticity diagram. The fluorescence emission ranges of the seven Nd-nanopaper@FB were between 425 and 550 nm (Fig. 5a). For the fluorescence of these seven Nd-nanopaper@FB under 311 nm excitation, the corresponding CIE values were Nd-nanopaper@FB1-(0.1665, 0.2346), Nd-nanopaper@FB2-(0.1825, 0.1765), Nd-nanopaper@FB3-(0.2005, 0.2677), Nd-nanopaper@FB4-(0.1854, 0.2002), Nd-nanopaper@FB5-(0.1659, 0.1529), Nd-nanopaper@FB6-(0.1601, 0.1449), and Nd-nanopaper@FB7-(0.1604, 0.0922; Fig. 5b). The fluorescent peaks of pure fluorescence brighteners were slightly different from the

fluorescent peaks of Nd-nanopaper@FB from 450 to 550 nm (Fig. S14). Some minor deviations occurred because fluorescent brightener addition to Nd-nanopaper inevitably caused some diffuse reflections and weak interaction. The up-converted Vis light fluorescence spectrum ($\lambda_{max} = 450$ nm) of Nd-nanopaper@FB at an excitation wavelength of 580 nm and the fluorescence intensity and peak position were similar (Fig. 5c). The up-conversion fluorescence of Nd-nanopaper@FB showed CIE coordinates that were all localized at (0.1542, 0.02; Fig. 5d). When irradiated separately under natural light, these Nd-nanopaper@FB samples did not fluoresce. However, under UV light at 365 nm, the seven fluorescent brighteners were excited, emitting blue fluorescence (Fig. 5e). Clearly, Nd-nanopaper and nanopaper@FB were colorless and without light emission under natural light. However, under the excitation of 365 nm ultraviolet light, the Nd-nanopaper emitted NIR luminescence (invisible to the naked eye), while nanopaper@FB emitted blue (Vis) fluorescence (Fig. S15).

As is known, fluorescent materials or FB are prone to photo-bleaching, when exposed to long-term ultraviolet radiation, and their molecular structure irreversibly damaged. NIR luminescence of Nd^{3+} ions originates from ligand sensitization, called the "antenna effect". Therefore, the longevity of Nd-MOFs and FB emitters under UV excitation depends on H_3BTC and FB's photostability, respectively. The UV absorption curves of a solution of the H_3BTC and representative FB3 were measured every 30 min 10 times and it was observed that neither H_3BTC nor FB3 absorbance decreased, which demonstrated the good photostability of H_3BTC and FB (Figs. S16–S17).

The security anti-counterfeiting model and its rules were studied based on switchable up and down-conversion luminescent properties of lanthanide-based cellulose nanopapers (Fig. 6) (Zhang, Chang et al., 2018, Zhang, Zhang et al., 2018). The detailed security code information was explained below. For the present Nd-nanopaper, it not only could produce down-conversion NIR fluorescence under excitation at 311 nm, but also emitted up-conversion Vis light under excitation at 580 nm. Thus, switchable dual-channel emission was achieved (Fig. 6a). For nanopaper@FB, it only emitted down-conversion Vis light under excitation at 311 nm (Fig. 6b). Nd-nanopaper@FB integrated the fluorescent characteristics of the above two nanopaper types (Fig. 6c). First, Nd-nanopaper@FB was excited by 311 nm, which generated a dual

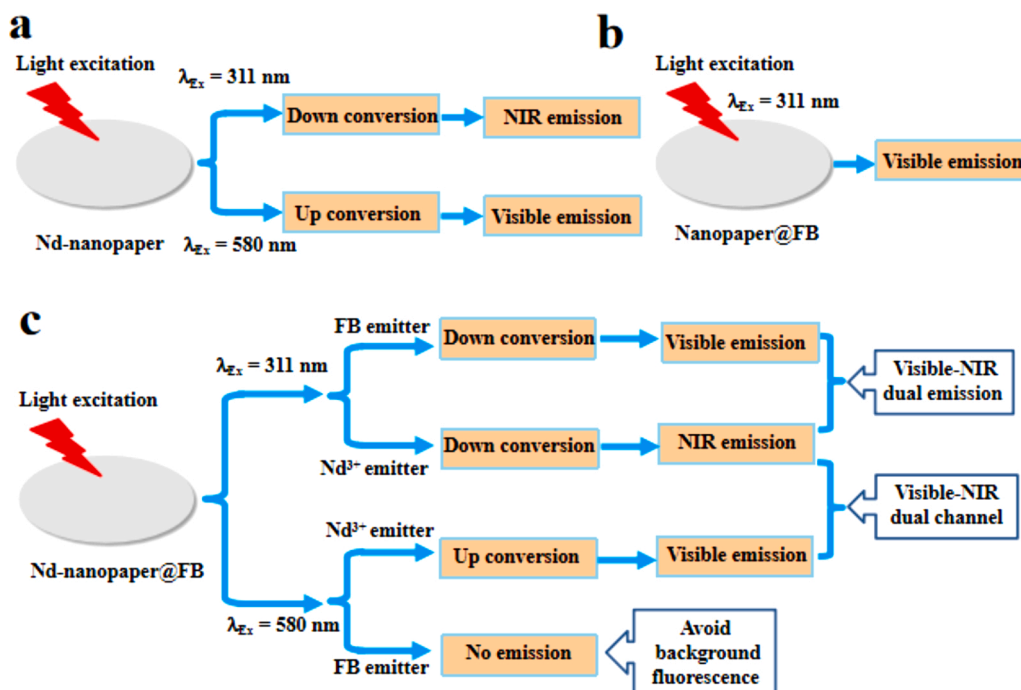


Fig. 6. The schematic illustration for anti-counterfeiting element and mechanism of Nd-nanopaper (a), nanopaper@FB (b) and Nd-nanopaper@FB (c).

emission. In the Vis region, fluorescent colors of fluorescent brighteners were able to be identified directly by the naked eye. Conversely, NIR luminescence could not be recognized with the naked eye and only detected using some advanced analytical instruments. Moreover, here, as both the fluorescent brightener excitation spectra (Fig. S18) and Nd³⁺ down-conversion NIR excitation spectrum overlapped in their absorption spectra (Fig. S19), fluorescent brightener Vis (450 nm) emissions and Nd³⁺ NIR (1060 nm) dual emission were generated under 311 nm excitation. Second, when Nd-nanopaper@FB was excited at 580 nm, only one band of fluorescence emission is produced, which meant that the naked eye could directly recognize the fluorescent of Nd³⁺ fluorescence in the Vis light region. The fluorescent brighteners did not fluoresce, which negated interference by background fluorescence from fluorescent brighteners. Therefore, the Nd³⁺ emitter generated up-converted fluorescence under 580 nm excitation and down-converted fluorescence under 311 nm excitation (Wang, Xie, Suehiro, Takeda, & Hirotsaki, 2018). Thereby, this material could be used in Vis and NIR dual emission and dual channel anti-counterfeiting applications.

4. Conclusions

These Nd-nanopapers were synthesized by a one pot solvothermal method. Shifting away from traditional down-conversion Vis emission anti-counterfeiting, the present Nd-nanopapers achieved down-conversion NIR emission and up-conversion Vis emission. The down-conversion luminescent property of Nd-nanopaper exhibited characteristic NIR luminescence ($\lambda_{Em} = 1080$ nm) of Nd³⁺ ions when excited by 311 nm, which underwent an “antenna” effect by the H₃BTC ligand. In contrast, up-conversion Vis light emission ($\lambda_{Em} = 450$ nm) of Nd-nanopaper was detected under 580 nm excitation, which was ascribed to excited-state absorption and energy transfer up-conversion. Nd-nanopaper induced both up and down-conversion for Vis and NIR emissions that completely avoided interference by fluorescent brighteners and background fluorescence. This switchable up and down-conversion fluorescent Nd-nanopaper with Vis and NIR dual emission or dual channel could be applied in high level anti-counterfeiting applications.

Declaration of Competing Interest

The authors declare that they have no conflict of interest.

Acknowledgments

This work was supported by National Natural Science Foundation of China (21703131, 31370578), Doctoral Scientific Research Foundation of Shaanxi University of Science & Technology (2016BJ-40), State Key Laboratory of Pulp and Paper Engineering, South China University of Technology (201821), Special Research Fund by Shaanxi Provincial Department of Education (18JK0122), Chinese Postdoctoral Science Foundation (2018M643707), Natural Science Basic Research Plan in Shaanxi Province of China (2019JQ-516), Guangxi Key Laboratory of Clean Pulp & Papermaking and Pollution Control (2019KF18, 2019KF33), State Key Laboratory of Biobased Material and Green Papermaking (KF201918).

Appendix A. Supplementary data

Supplementary material related to this article can be found, in the online version, at doi:<https://doi.org/10.1016/j.carbpol.2020.117134>.

References

Abraham, E., Kam, D., Nevo, Y., Slattegard, R., Rivkin, A., Lapidot, S., & Shoseyov, O. (2016). Highly modified cellulose nanocrystals and formation of

- epoxy nanocrystalline cellulose (CNC) nanocomposites. *ACS Applied Materials & Interfaces*, 8(41), 28086–28095.
- Andres, J., Hersch, R. D., Moser, J., & Chauvin, A. (2014). A new anti-counterfeiting feature relying on invisible luminescent full color images printed with lanthanide-based inks. *Advanced Functional Materials*, 24(32), 5029–5036.
- Arppe, R., & Sørensen, T. J. (2017). Physical unclonable functions generated through chemical methods for anti-counterfeiting. *Nature Reviews Chemistry*, 1(4), 1–13.
- Chen, Y., Geng, B., Jing, R., Tong, C., & Chen, J. (2017). Comparative characteristics of TEMPO-oxidized cellulose nanofibers and resulting nanopapers from bamboo, softwood, and hardwood pulps. *Cellulose*, 24(11), 1–14.
- Chuang, T., & Verdun, H. R. (1996). Energy transfer up-conversion and excited state absorption of laser radiation in Nd:YLF laser crystals. *IEEE Journal of Quantum Electronics*, 32(1), 79–91.
- Courrol, L. C., Lima, B. L. S. D., Kassab, L. R. P., Cacho, V. D. D., Tatum, S. N. H., Gomes, L., et al. (2004). Up-conversion losses in Nd³⁺ doped lead fluoroborate glasses. *Journal of Non-Crystalline Solids*, 348(15), 98–102.
- Da Luz, L. L., Milani, R., Felix, J. F., Ribeiro, I. R. B., Talhavin, M., Neto, B. A. D., et al. (2015). Inkjet printing of lanthanide-organic frameworks for anti-counterfeiting applications. *ACS Applied Materials & Interfaces*, 7(49), 27115–27123.
- Dexter, D. L. J. (1953). A theory of sensitized luminescence in solid. *Journal of Chemical Physics*, 21(5), 836–850.
- Foster, E. J., Moon, R. J., Agarwal, U. P., Bortner, M. J., Bras, J., Camarero-Espinosa, S., et al. (2018). Current characterization methods for cellulose nanomaterials. *Chemical Society Reviews*, 47(8), 2609–2679.
- Gao, Z., Han, Y., & Wang, F. (2018). Cooperative supramolecular polymers with anthracene–endoperoxide photo-switching for fluorescent anti-counterfeiting. *Nature Communications*, 9(1), 3977.
- Jing, K., Sun, S., Zhang, L., Lu, Y., Wu, A., Cai, C., et al. (2015). Red, green, and blue luminescence by carbon dots: full-color emission tuning and multicolor cellular imaging. *Angewandte Chemie International Edition*, 54(18), 5360–5363.
- Jiang, K., Zhang, L., Lu, J., Xu, C., Cai, C., & Lin, H. (2016). Triple-Mode emission of carbon dots: applications for advanced anti-counterfeiting. *Angewandte Chemie International Edition*, 55(25), 7231–7235.
- Jin, L., Dong, Z., Mei, S., Yu, Y. F., Wei, Z., Pan, Z., et al. (2018). Noninterleaved metasurface for (26-1) spin- and wavelength-encoded holograms. *Nano Letters*, 18(12), 8016–8024.
- Kaczmarek, A. M., Liu, Y., Wang, C., Laforce, B., Vincze, L., Van Der Voort, P., et al. (2017). Lanthanide “chameleon” multistage anti-counterfeit materials. *Advanced Functional Materials*, 27(20), Article 1700258.
- Leng, T., Jakubek, Z. J., Mazloumi, M., Leung, A. C. W., & Johnston, L. J. (2017). Ensemble and single particle fluorescence characterization of dye-labeled cellulose nanocrystals. *Langmuir*, 33(32), 8002–8011.
- Li, X., Xie, Y., Song, B., Zhang, H., Chen, H., Cai, H., et al. (2017). A stimuli-responsive smart lanthanide nanocomposite for multidimensional optical recording and encryption. *Angewandte Chemie International Edition*, 56(10), 2689–2693.
- Lin, N., & Dufresne, A. (2014). Surface chemistry, morphological analysis and properties of cellulose nanocrystals with gradiented sulfation degrees. *Nanoscale*, 6(10), 5384–5393.
- Liu, Y., Ai, K., & Lu, L. (2011). Designing lanthanide-doped nanocrystals with both up and down-conversion luminescence for anti-counterfeiting. *Nanoscale*, 3(11), 4804–4810.
- Lupei, V., & Lupei, A. (2000). Emission dynamics of the ⁴F_{3/2} level of Nd³⁺ in YAG at low pump intensities. *Phys. Rev. B*, 61(12), 8087–8098.
- Missoum, K., Bras, J., & Belgacem, M. N. (2012). Organization of aliphatic chains grafted on nanofibrillated cellulose and influence on final properties. *Cellulose*, 19(6), 1957–1973.
- Miao, M., Zhao, J., Feng, X., Cao, Y., Cao, S., Zhao, Y., et al. (2015). Fast fabrication of transparent and multi-luminescent TEMPO-oxidized nanofibrillated cellulose nanopaper functionalized with lanthanide complexes. *Journal of Materials Chemistry C*, 3(11), 2511–2517.
- Resch-Genger, M. S. J. K. (2020). Near-IR to Near-IR upconversion luminescence in molecular chromium ytterbium salts. *Angewandte Chemie-International Edition*. <https://doi.org/10.1002/anie.202007200>
- Santos, M. D. L., Batlle, R., Salafranca, J., & Nerin, C. (2005). Subcritical water and dynamic sonication-assisted solvent extraction of fluorescent whitening agents and azo dyes in paper samples. *Journal of Chromatography A*, 1064(2), 135–141.
- Sato, S., & Wada, M. (1970). Relations between intramolecular energy transfer efficiencies and triplet state energies in rare earth β -diketone chelates. *Bulletin of the Chemical Society of Japan*, 43, 1955–1962.
- Shu, W. C., & Ding, W. H. (2009). Determination of fluorescent whitening agents in infant clothes and paper materials by ion-pair chromatography and fluorescence detection. *Journal of the Chinese Chemical Society*, 56(4), 797–803.
- Tai, Y., Li, X., & Pan, B. (2018). Efficient near-infrared down conversion in Nd³⁺-Yb³⁺ co-doped transparent nanostructured glass ceramics for photovoltaic application. *Journal of Luminescence*, 195, 102–108.
- Wang, H. Q., Batentschuk, M., Osvet, A., Pinna, L., & Brabec, C. J. (2011). Rare-earth ion doped up-conversion materials for photovoltaic applications. *Advanced Materials*, 23(22-23), 2675–2680.
- Wang, J., Song, B., Tang, J., Hu, G., Wang, J., Cui, M., et al. (2020). Multi-modal anti-counterfeiting and encryption enabled through silicon-based materials featuring pH-responsive fluorescence and room-temperature phosphorescence. *Nano Research*, 13(6), 1614–1619.
- Wang, L., Xie, R. J., Suehiro, T., Takeda, T., & Hirotsaki, N. (2018). Down-conversion nitride materials for solid state lighting: recent advances and perspectives. *Chemical Reviews*, 118(4), 1951–2009.

- Wang, P., Xia, H., Peng, J., Hu, H., Lei, T., Zhang, Y., et al. (2014). Concentration effect of Nd^{3+} ion on the spectroscopic properties of $\text{Er}^{3+}/\text{Nd}^{3+}$ co-doped LiYF_4 single crystal. *Materials Chemistry & Physics*, *144*(3), 349–354.
- You, M., Lin, M., Wang, S., Wang, X., Zhang, G., Hong, Y., et al. (2016). Three-dimensional quick response code based on inkjet printing of upconversion fluorescent nanoparticles for drug anti-counterfeiting. *Nanoscale*, *8*(19), 10096–10104.
- Zhang, S., Liu, G., Chang, H., Li, X., & Zhang, Z. (2019). Optical haze nanopaper enhanced ultraviolet harvesting for direct soft-fluorescent emission based on lanthanide complex assembly and oxidized cellulose nanofibrils. *ACS Sustainable Chemistry & Engineering*, *7*(11), 9966–9975.
- Zhang, Z., Chang, H., Xue, B., Zhang, S., Li, X., Wong, W., et al. (2018). Near-infrared and visible dual emissive transparent nanopaper based on Yb(III)-carbon quantum dots grafted oxidized nanofibrillated cellulose for anti-counterfeiting applications. *Cellulose*, *25*(1), 377–389.
- Zhang, Z., Chen, Z., Sun, L., Zhang, X., & Zhao, Y. (2019). Bio-inspired angle-independent structural color films with anisotropic colloidal crystal array domains. *Nano Research*, *12*(7), 1579–1584.
- Zhang, Z., Zhang, M., Li, X., Li, K., Lü, X., Wang, Y., et al. (2018). Irreversible solvatochromic Zn-nanopaper based on Zn(II) terpyridine assembly and oxidized nanofibrillated cellulose. *ACS Sustainable Chemistry & Engineering*, *6*(9), 11614–11623.
- Zhao, J., Wei, Z., Feng, X., Miao, M., Sun, L., Cao, S., et al. (2014). Luminescent and transparent nanopaper based on rare-earth up-converting nanoparticle grafted nanofibrillated cellulose derived from garlic skin. *ACS Applied Materials & Interfaces*, *6*(17), 14945–14951.
- Zhu, S., Zhang, J., Tang, S., Qiao, C., Wang, L., Wang, H., et al. (2012). Surface chemistry routes to modulate the photoluminescence of graphene quantum dots: from fluorescence mechanism to up-conversion bioimaging applications. *Advanced Functional Materials*, *22*(22), 4732–4740.
- Zor, E., Alpaydin, S., Arici, A., Saglam, M. E., & Bingol, H. (2017). Photoluminescent nanopaper-based microcuvette for iodide detection in seawater. *Sensors & Actuators B Chemical*, *254*, 1216–1224.